NARX Models of an Industrial Power Plant Gas Turbine

M. Basso, L. Giarré, S. Groppi, and G. Zappa

***Abstract*—This brief reports the experience with the identification of a nonlinear autoregressive with exogenous inputs (NARX) model for the PGT10B1 power plant gas turbine manufactured by General Electric-Nuovo Pignone. Two operating conditions of the turbine are considered: isolated mode and nonisolated mode. The NARX model parameters are estimated iteratively with a Gram–Schmidt procedure, exploiting both forward and stepwise regression. Many indexes have been evaluated and compared in order to perform subset selection in the functional basis set and determine the structure of the nonlinear model. Various input signals (from narrow to broadband) for identification and validation have been considered.**

***Index Terms*—Gas turbines, identification, modeling, nonlinear systems, power systems, turbines.**

I. Introduction

TODAY'S industrial gas and steam turbines are designed to be more energy-efficient, more reliable, and longer-lived than their predecessors. The General Electric-Nuovo Pignone PGT10 is a small heavy-duty high efficiency gas turbine (generating up to 11 MW of power). In our application setup, the PGT10B1 turbine was employed as generator drive, operating either as a stand-alone unit, disconnected from an external power grid (isolated mode), or connected to an external power grid (nonisolated mode).

Gas turbine generators are often connected to small supply systems. Since system disturbances arising from faults or load fluctuations could drive these generators to instability, there is an increasing demand for accurate dynamical models, in order to investigate the system response to disturbances and improve existing control loops [10], at least for standard operating conditions (namely, full speed and variable load). Based on the thermo-fluid physical laws GE-Nuovo Pignone usually develops continuous-time, high-order nonlinear dynamical models (GT systems, in the sequel), whose accuracy is validated through experimental tests on real plants in various operating conditions. Unfortunately, such models present a very high computational complexity. On the other hand, the transient and long-term behavior of the overall power system is studied through computer simulations of the interconnected network formed by generators, loads, and transmission lines.

Manuscript received January 20, 2003. Manuscript received in final form April 21, 2004. Recommended by Associate Editor A. Isaksson.

M. Basso is with Dipartimento di Sistemi e Informatica, Università di Firenze, I-50139 Firenze, Italy (e-mail: basso@dsi.unifi.it).

G. Zappa, deceased, was with Dipartimento di Sistemi e Informatica, Università di Firenze, I-50139 Firenze, Italy.

L. Giarré is with Dipartimento di Ingegneria dell'Automazione e dei Sistemi, Università di Palermo, I-90128 Palermo, Italy (e-mail: giarre@unipa.it).

S. Groppi is with General Electric-Nuovo Pignone, I-50127 Firenze, Italy (e-mail: Stefano.Groppi@np.ge.com).

Digital Object Identifier 10.1109/TCST.2004.843129

TABLE I
NOMENCLATURE AND ACRONYMS

ARX	Auto Regressive with eXogenus input
NARX	Nonlinear Auto Regressive with eXogenus input
NARMAX	Nonlinear Auto Regressive Moving Average with eXogenus input
SISO	Single Input Single Output
MISO	Multiple Input Single Output
LS	Least Squares
FPE	Final Prediction Error
GT	Gas Turbine
FSR	Fuel Stroke Reference
T	Generated Torque
Te	Load Torque
WF	Fuel Flow
VEL	Turbine Angular Velocity

Since the simulation computational burden is highly dependent on the complexity and accuracy of each generator model, the customer often requires a reliable low-complexity prototype model of the gas-turbine generator set, sufficiently accurate for the previous application [12].

The aim of the present work is to buildup a reduced order accurate nonlinear dynamical model of the gas turbine exploiting black-box identification techniques. Previous work on identification of gas turbine dynamics mainly concerned aircraft gas turbine engines. SISO models of the fuel-flow turbine-speed relation were obtained using a variety of identification methods: frequency domain techniques, linear parametric varying models, NARMAX models, multiobjective optimization (see [2] and [3] for a comprehensive survey). In this brief, both SISO and MISO models will be identified exploiting time-domain techniques. Moreover, polynomial NARX models have been adopted since

1) they can well approximate many nonlinear dynamical systems [11] and exhibit a wide range of nonlinear dynamical behaviors [5];
2) the parameter estimation task is trivial.

However, since the functional relation among present output and past I/O data is usually unknown and a set of basis functions must be selected in order to reproduce this relation within an acceptable accuracy, efficient techniques must be employed in order to limit the complexity of the model and to avoid overfitting. The purpose of this brief is twofold: first to show that NARX models can be easily identified and outperform linear models (ARX) [13] in describing gas turbine dynamics over the full operating range. Second, to investigate, exploiting this case-study, the effectiveness of several complexity selection techniques for black-box nonlinear modeling in order to get conclusions of general validity.

II. NARX Model Identification and Structure Selection

Preliminary identification experiments of the GT system, exploiting step inputs of different amplitude, showed that the steady-state input–output relation is essentially linear. Conversely, identification of low dimensional linear models around different operating points provided models heavily dependent on the selected operating point. This is apparent in the poles locus of the identified models (Fig. 1). Hence, a single linear model cannot adequately describe the GT system dynamics over the full operating range. However, since the dc-gain is approximately constant, the nonlinear behavior of the GT system cannot be explained by a static nonlinear block as in Wiener–Hammerstein models and more general nonlinear models must be adopted.

In this brief, NARX models have been considered for black-box identification. A NARX model $\mu(\theta)$ is characterized by the one-step ahead predictor

$$\hat{y}(t\,|\,\theta) = F(\psi(t)) \tag{1}$$

where the vector $\psi(t) = [y(t-1), \ldots, y(t-n), u(t-1), \ldots, u(t-m)]$ represents the memory of the model and $F(\cdot): \Re^{n+m} \rightarrow \Re$. Since the function F is, to a large extent, unknown it is approximated by an expansion in a given function basis. In polynomial NARX models

$$F(\psi(t)) \cong \sum_{i=1}^{n_\theta} \theta_i \phi_i(t) \tag{2}$$

where $\phi_i(t)$ are monomials, of degree less or equal to l, in the variables contained in $\psi(t)$ and θ_i are the corresponding expansion coefficients. Hence, the one-step prediction assumes the standard regression form

$$F(\psi(t)) \cong \phi(t)\theta \tag{3}$$

where $\theta = [\theta_1, \ldots, \theta_{n_\theta}]^T$ is the parameter vector, and $\phi(t) = [\phi_1(t), \ldots, \phi_{n_\theta}(t)]$ the regressor. Therefore, predictions are linear in the parameters and, given $\phi(t)$, the minimum prediction error estimate $\hat{\theta}$ can be easily obtained by an LS algorithm.

The crucial point in NARX modeling is the determination of the structure of the regressor. Notice that the index vector $[n, m, l]$, which is usually fixed *a priori*, defines a family of models (3). Since the maximum number of monomials that could be included in $\phi(t)$ is very large, i.e., $n_{\max} = \sum_{k=0}^{l} \binom{n+m+k-1}{k}$, effective techniques must be adopted in order to limit the complexity n_θ of the model and avoid overfitting. In this brief, several procedures discussed in [4], [9], and [14] have been implemented and compared.

The whole identification experiment can be summarized as follows:

1) Data Collection: I/O data are collected and the data set is divided in identification $\mathcal{D}_i$ and validation $\mathcal{D}_v$ subsets with cardinality N_i and N_v, respectively.

2) Parameter Identification: For each model structure, the LS estimate $\hat{\theta}$ is computed on the identification data subset $\mathcal{D}_i$ using a Gram–Schmidt procedure [9].

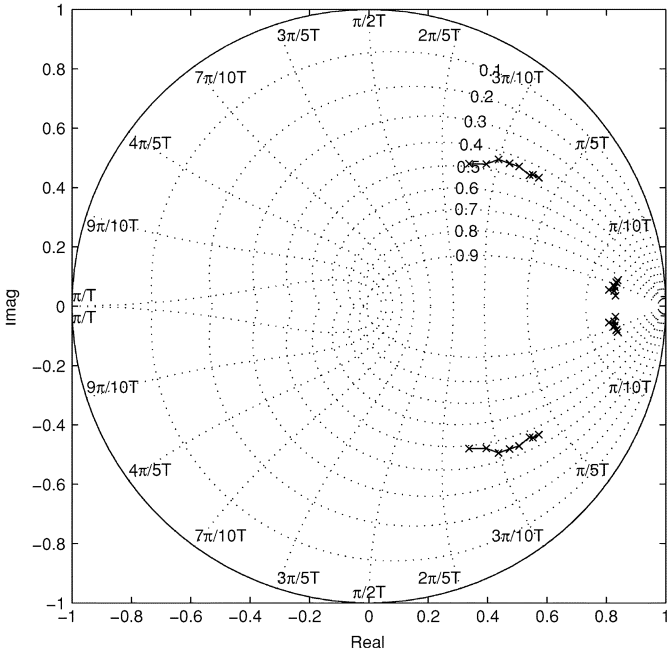

Fig. 1. Analysis of the dynamics of the linear models: poles locus corresponding to different opening percentage of the valve (from 35% to 70%).

3) Structure Selection: For each identified model $\mu(\hat{\theta})$, the cost functional

$$J(\hat{\theta}) = \frac{1}{N_{\mathcal{D}}} \sum_{t \in \mathcal{D}} \varepsilon^2(t\,|\,\hat{\theta}) \left(1 + \frac{\beta(\hat{\theta})}{N_i}\right) \tag{4}$$

is evaluated, where

- $\varepsilon(t\,|\,\theta)$ is either the prediction $\varepsilon_p(t\,|\,\theta) \doteq y(t) - \phi(t)\theta$ or the simulation error $\varepsilon_s(t\,|\,\theta) \doteq y(t) - \hat{\phi}(t\,|\,\theta)\theta$, being $\hat{\phi}(t\,|\,\theta)$ the pseudo-regressor in which the actual output values have been replaced by their "predictions" provided by the model itself;
- $\mathcal{D} = \mathcal{D}_i$ or $\mathcal{D} = \mathcal{D}_v$, with cardinality $N_{\mathcal{D}}$;
- $\beta(\theta)$ is a term penalizing the complexity of the model which may assume the following values:

$$\beta(\theta) = \begin{cases} 0 \\ 2n_\theta \\ 2n_{\text{eff}} \end{cases} \tag{5}$$

where n_{eff} is the sum of the degrees of the monomials in ϕ.

The model with minimum $J(\hat{\theta})$ is preferred.

4) Search Strategies: Since, for computational reasons, it is not possible to evaluate J for all structures of a given complexity, suboptimal search strategies are adopted. In particular, according to [6] and [8], we considered the following.

- *Forward Strategy*. Starting from the empty regressor, at each step of the iterative procedure the monomial which yields the maximum decrease of J is inserted in ϕ.
- *Stepwise Strategy*. At each step, after a new monomial has been inserted in the regressor according to the forward strategy, a monomial is also removed from ϕ if this provides a decrease of J.

The search procedure terminates when a cost decrease cannot be further obtained. Forward and stepwise strategies are clearly suboptimal leading to a local minimum of J.

5) Validation: Identified models are validated exploiting linear and nonlinear correlation tests among model residuals and I/O variables [14].

6) Performance Evaluation: The quality of identified models is assessed by computing the sample variance of the model prediction and simulation errors on new data. In particular, data produced by input signals with different spectral characteristic w.r.t. signals employed in the identification and structure selection steps.

Remark 1: The cost-functional $J(\theta)$ encompasses, with its several options, many structure selection procedures. In particular, when $\varepsilon = \varepsilon_p, \mathcal{D} = \mathcal{D}_i$ and $\beta(\hat{\theta}) \neq 0$ we get the FPE criterium, suitable modified for weighting nonlinear terms. When $\mathcal{D} = \mathcal{D}_v$ and $\beta = 0$ we get the cross validation approach to structure selection [13]. The use of the simulation error in J [4] deserves a specific comment. It should be noticed that, since the ultimate goal of the identified model is the *simulation* of the GT system dynamics in the stability analysis of interconnected power plants, identification should be based on the minimization of the *simulation* rather than *prediction* error. However this leads to a nonconvex optimization problem, which cannot be easily solved. Consequently, simulation errors are only exploited for model structure selection whereas parameters are estimated by minimizing the prediction error.

The previous selection procedure is automatic and does not require any subjective choice by the human operator. Only when $\beta = 0, \varepsilon = \varepsilon_p$, and $\mathcal{D} = \mathcal{D}_i$, some heuristics must be adopted in order to bound the number of terms in the regressor.

Remark 2: The forward and stepwise strategies select, at each step, the most explicative monomial and induce, in some sense, an ordering relation among them. Obviously this is not entirely correct since the selection of the new monomial is conditioned to the monomial basis already selected in previous steps. A true ordering is obtained only when the information matrix is orthogonal. However, the order in which monomials are selected has a certain significance.

III. Discussions of the Results

A schematic of the main blocks of the GT system is reported in Fig. 2, where only the inputs, outputs, and connections of interest for the present work are shown.

- *Gas System Block*—This block models the turbine actuator dynamics: valves, servovalves, servomechanisms. Its main input is the FSR, the opening percentage of the fuel valve, whereas the output is the fuel flow WF. The dynamics also depends on the turbine angular velocity.
- *Turbine Block*—This block reproduces the compressor, combustion, and expansion chamber dynamics. The input of this block is the fuel flow, the output is the generated torque T. The model dynamics also depends on the turbine angular velocity VEL.
- *Load Block*—In nonisolated mode this block computes the generated power PW as the product of the exogenous grid angular velocity and the generated torque T. In isolated mode, this block computes the angular velocity on the basis of the load torque T_e, the generated torque T, and the turbine mechanical parameters (inertia, friction, etc.).
- *Control Block*—In standard operating conditions, two different controller schemes can be selected: 1) in isolated mode, the turbine supplies power directly to a specific electrical load and the frequency need to be regulated (*droop controller*); 2) in nonisolated mode, the frequency is fixed by the external grid while the power need to be regulated (*isochronous controller*).

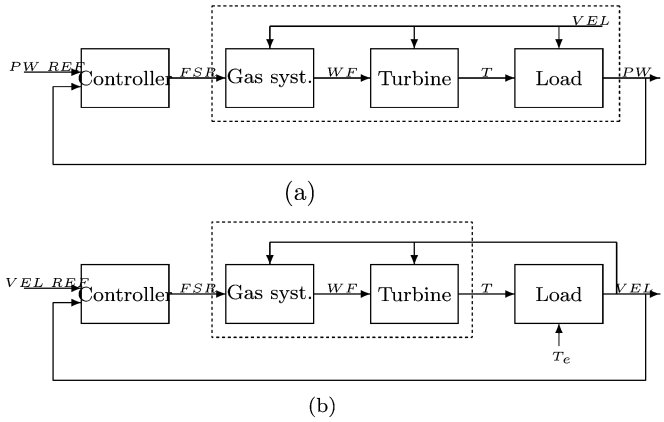

Fig. 2. Schematic of the Gas turbine system. (a) Nonisolated operating mode. (b) Isolated operating mode.

GT system identification results are reported hereafter, considering both nonisolated and isolated turbine operating modes. A sampling time $T_s = 0.05$ s has been adopted, corresponding to $1/4$ of the plant rising time in response to a step of the FSR around the 50% operating point. In each experiment, 3000 I/O samples have been collected and the mean subtracted. The first 1800 samples constitute the identification subset. Three kinds of input signals with different power spectrum have been considered, namely: narrow-band signals (e.g., multisine); middle-band signals (e.g., square or triangular waves); and wide-band signals (three level signals with small amplitude white noise superimposed). Not surprisingly the performance of identified models improves, i.e., the sample variance of prediction and simulation errors decreases when they are evaluated on data generated by input signals similar to those exploited for the identification step. There is however a noticeable exception: models identified exploiting wide-band input signals have better performances even for narrow or middle-band input signals. This is in good agreement with what was observed in [2].

The structure selection procedures considered in the identification experiments are summarized in Table II.

A. Nonisolated Mode

In nonisolated mode the frequency is fixed (50 Hz); aim of the identification procedure is to identify a SISO model of the gas-system and turbine blocks where the only input signal $u(t)$ is the FSR and the output signal $y(t)$ is the generated power PW, [see the dashed-line box in Fig. 2(a)]. Identification is carried out in open loop, i.e., the control block is disconnected and the FSR profile is selected by the user.

TABLE II
STRUCTURE SELECTION PROCEDURES

Procedure	$\varepsilon_p/\varepsilon_s$	$\mathcal{D}_i/\mathcal{D}_v$	β
1	ε_p	$\mathcal{D}_i$	0
2	ε_p	$\mathcal{D}_i$	$2n_\theta$
3	ε_p	$\mathcal{D}_i$	$2n_{eff}$
4	ε_s	$\mathcal{D}_v$	0
5	ε_s	$\mathcal{D}_v$	$2n_\theta$
6	ε_s	$\mathcal{D}_v$	$2n_{eff}$
7	ε_p	$\mathcal{D}_v$	0
8	ε_p	$\mathcal{D}_v$	$2n_\theta$
9	ε_p	$\mathcal{D}_v$	$2n_{eff}$

TABLE III
COMPLEXITY AND PERFORMANCES OF THE IDENTIFIED MODELS

Procedure	n_θ	n_{eff}	$\sigma^2(\varepsilon_p)$ $[KW^2]$	$\sigma^2(\varepsilon_s)$ $[KW^2]$
1	30	72	0.473×10^3	11.49×10^3
2	22	54	0.446×10^3	9.73×10^3
3	18	42	0.462×10^3	8.17×10^3
4-5	18	34	0.277×10^3	5.77×10^3
6	13	24	0.272×10^3	6.06×10^3
7	29	60	0.549×10^3	9.83×10^3
8	26	51	0.572×10^3	10.89×10^3
9	13	19	0.280×10^3	8.99×10^3

The following complexity indexes where adopted: $n = 3$, $m = 3, l = 3$. In particular, the last choice allows quadratic and cubic nonlinearities. Each identification procedure provided a model. Their prediction and simulation capabilities were subsequently evaluated exploiting various kind of input signals with different frequency content. In Table III complexity and performances of identified models are reported (procedures 4 and 5 giving the same model). Models were identified on data generated by broadband signals while errors refer to narrow-band signals. Performances are evaluated in terms of the sample variances $\sigma^2(\varepsilon_p)$ and $\sigma^2(\varepsilon_s)$ of prediction and simulation errors, respectively.

It is evident from this table that the models selected by weighting ε_s (procedures 4–6) have less complexity and provide better performance. Due to space limitations we report in Table IV the model obtained with procedures 4–5 only, where $\bar{u} \doteq 100(u - u_m)$ and $\bar{y} \doteq 10^{-3}(y - y_m)$, being $u = \text{FSR} \in [0, 1]$, with $u_m = 0.5674$, and the generated power y expressed in KW, with $y_m = 7714$ [KW]. This model perfectly fits the system dc-gain at different operating points.

By comparing the coefficients and the structure of the different identified models some conclusions can be derived.

- In all models, the leading terms in the regressor are the linear ones.
- The use of different weights β modifies the number of selected monomials, not their order in the regressor. Moreover, adding new monomials to the regressor does not significantly modify the coefficient estimates of the previous monomials. This means that the input signals are sufficiently rich to ensure a well conditioned information matrix.

TABLE IV
NONISOLATED MODE: NARX MODEL OBTAINED WITH PROCEDURES 4–5

$\hat{\theta}_i$	$\phi_i(t)$
-40.251	$\bar{u}(t-3)$
-146.2	$\bar{y}(t-3)$
62.391	$\bar{u}(t-1)$
1.056	$\bar{y}(t-1)$
-17.92	$\bar{u}(t-2)$
0.0136	$\bar{u}^2(t-1)$
11.46	$\bar{y}(t-2)\bar{u}(t-2)$
69.5	$\bar{y}(t-2)$
1.002	$\bar{y}^3(t-3)$
3.901	$\bar{y}^2(t-2)\bar{u}(t-3)$
-3.50	$\bar{y}(t-2)\bar{y}(t-3)\bar{u}(t-3)$
-0.9818	$\bar{y}(t-3)\bar{u}(t-2)$
-2.4931	$\bar{y}^3(t-2)$
-6.0908	$\bar{y}^2(t-1)$
-0.3591	$\bar{u}(t-1)\bar{u}(t-3)$
1.274	$\bar{y}(t-3)\bar{u}(t-3)$
0.5382	1
-0.01878	$\bar{y}(t-3)\bar{u}(t-2)\bar{u}(t-3)$

- Conversely, models selected using prediction errors ε_p differ substantially from models selected using simulation errors ε_s since they have the following.
  1) Different number of monomials (the ε_s-based models have less parameters).
  2) Different ordering of monomials (the ε_s-based models have more input than output terms in the regressor). This agrees with what was noticed in [4] for a different application of NARX models identification.

1) Validation: According to [1], the following correlation statistics have been computed:

$$\phi_{\varepsilon\varepsilon}(\tau) = \frac{\sum_{t\in\mathcal{D}_i} \bar{\varepsilon}_p(t)\bar{\varepsilon}_p(t-\tau)}{\sum_{t\in\mathcal{D}_i} \bar{\varepsilon}_p^2(t)}$$

$$\phi_{\varepsilon u}(\tau) = \frac{\sum_{t\in\mathcal{D}_i} \bar{\varepsilon}_p(t)\bar{u}(t-\tau)}{\sqrt{\sum_{t\in\mathcal{D}_i} \bar{\varepsilon}_p^2(t) \sum_{t\in\mathcal{D}_i} \bar{u}^2(t)}}$$

$$\phi_{\alpha\varepsilon^2}(\tau) = \frac{\sum_{t\in\mathcal{D}_i} \bar{\alpha}(t)\bar{\varepsilon_p}^2(t-\tau)}{\sqrt{\sum_{t\in\mathcal{D}_i} \bar{\alpha}^2(t) \sum_{t\in\mathcal{D}_i} \left(\bar{\varepsilon_p}^2(t)\right)^2}}$$

$$\phi_{\alpha u^2}(\tau) = \frac{\sum_{t\in\mathcal{D}_i} \bar{\alpha}(t)\bar{u}^2(t-\tau)}{\sqrt{\sum_{t\in\mathcal{D}_i} \bar{\alpha}^2(t) \sum_{t\in\mathcal{D}_i} (\bar{u}^2(t))^2}}$$

where $\alpha(t) = y(t)\varepsilon_p(t)$ and $\bar{}$ denotes deviation from the sample mean. In the ideal case where the prediction errors are zero mean and uncorrelated with all linear and nonlinear combinations of past input and outputs, these tests yield

$$\lim_{N_i\to\infty} \phi_{\varepsilon\varepsilon}(\tau) = 0, \qquad \tau \neq 0$$

$$\lim_{N_i\to\infty} \phi_{\varepsilon u}(\tau) = \lim_{N_i\to\infty} \phi_{\alpha u^2}(\tau) = 0, \qquad \forall\tau$$

$$\lim_{N_i\to\infty} \phi_{\alpha\varepsilon^2}(\tau) = \begin{cases} \text{const.}, & \tau = 0 \\ 0 & \tau \neq 0. \end{cases}$$

These tests detect linear and nonlinear terms appearing in the prediction errors, corresponding to missing terms in the model.

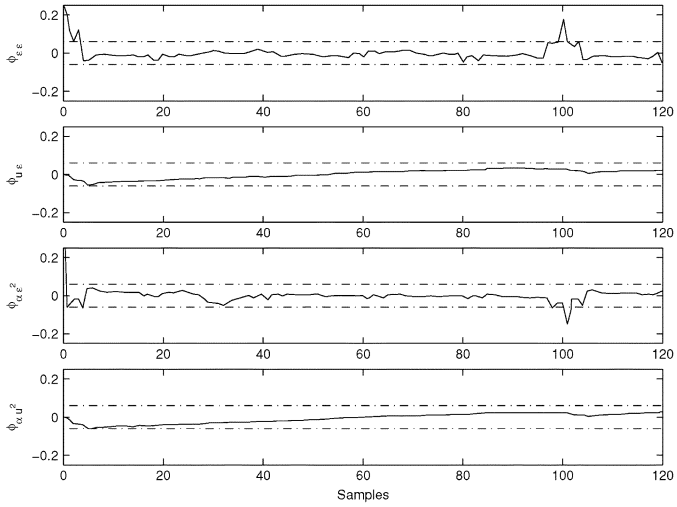

Fig. 3. Correlation tests for the best NARX models (procedure 4–5) in nonisolated mode.

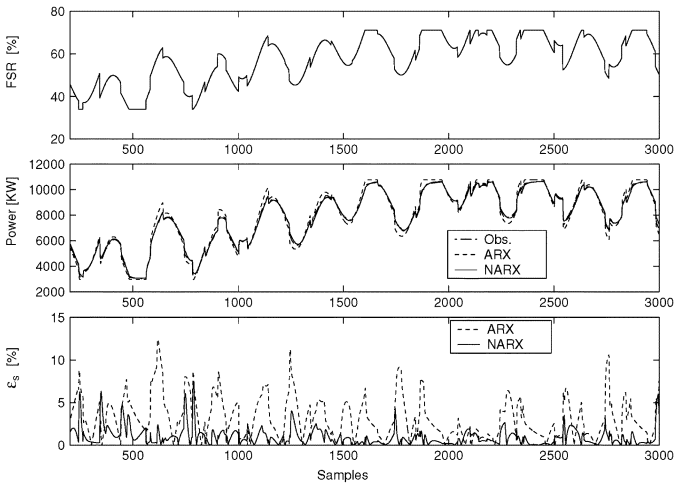

Fig. 4. Nonisolated mode. Comparison between NARX and ARX models. (a) Input signal. (b) Observed and simulated outputs. (c) Relative simulation errors.

The evaluation of the previous correlation statistics applied to the best NARX model are reported in Fig. 3 together with their 95% confidence interval. It turns out that prediction errors are uncorrelated with the input signal for any lag while prediction errors are weakly autocorrelated for time lags $\tau = 1$–3 and $\tau \simeq 100$. This is probably due to the intrinsic limitations of NARX models in describing the noise features.

Finally, NARX models have been compared with a linear ARX model, identified in a neighborhood of 50% FSR. The ARX structure is [4, 4, 1]. The linear model performance deteriorates especially for nonsmooth inputs. This is clearly indicated in Fig. 4, where simulated outputs and relative simulation errors are compared for the linear and the best nonlinear model.

B. Isolated Mode

The serial interconnection of the gas system and turbine blocks has two inputs (namely, FSR and VEL) and one output (the generated torque T), as shown by the dashed-line box in Fig. 2(b). However, since in normal operating conditions the velocity is correlated with the external load T_e and T, it is not convenient to carry out identification experiments in open loop, by varying arbitrarily and independently both inputs. In this case, the velocity would assume values exciting nonlinear dynamics which are not present in normal operating conditions. Hence, closed-loop identification experiments must be carried out, inserting the control block, while different operating conditions and external excitation are obtained by varying T_e. Identification in closed loop is accomplished using the direct approach [7]. Consequently, the identification task presents two additional difficulties:

1) the model is now MISO and much more terms can be inserted in the regressor;
2) input signals are correlated with past outputs, thus, inducing identifiability problems.

In a first stage, the MISO model was decoupled in two parallel SISO models, and only the model describing the velocity–torque relation was identified exploiting the previous identified model for the FSR–torque relation. Unfortunately, identification results were unsatisfactory, showing that the action of the two inputs is nonlinearly coupled.

Subsequently, fully connected MISO models were identified following the procedures previously indicated with complexity indexes $n = 3, m_1 = 3, m_2 = 3, l = 3$. Despite the previous difficulties, satisfactory MISO models were obtained, presenting small prediction and simulation errors. Once again the best model was obtained with procedure 5. Its structure and parameters are reported in Table V, in the variables $\bar{u} \doteq (u - u_m), \bar{v} \doteq 10(v - v_m)$, and $\bar{y} \doteq (y - y_m)$, where $u = \text{FSR} \in [0, 1]$, with $u_m = 0.5251$, the normalized angular velocity $v = \text{VEL}/50$, with $v_m = 1$, and the normalized generated torque $y = T/35.75$, with $y_m = 0.6315$.

Performance evaluation with various input signals has been performed. A comparison with an ARX model of structure [4, 4, 4, 1], identified in a neighborhood of 50% of the FSR valve and shaft rotational speed of 50 Hz, was also considered. In Fig. 5, the relative simulation error (in absolute value) is shown for the two NARX and ARX identified models. Once again the NARX model outperforms the linear one, since the relative simulation error never exceeds 3% for the former while it rises up

TABLE V
ISOLATED MODE: NARX MODEL OBTAINED WITH PROCEDURE 5

$\hat{\theta}_i$	$\phi_i(t)$
-0.3526	$\bar{u}(t-2)$
-1.732	$\bar{v}(t-2)$
-60.04	$\bar{v}^3(t-2)$
4.085	$\bar{v}(t-1)\bar{v}(t-3)$
0.003388	1
-0.0434	$\bar{y}(t-3)\bar{u}(t-1)$
-26.11	$\bar{u}(t-1)\bar{v}(t-1)\bar{v}(t-3)$
13.57	$\bar{u}(t-1)\bar{v}^2(t-2)$
2.364	$\bar{v}(t-1)$
0.2017	$\bar{y}(t-3)$
-15.32	$\bar{u}^2(t-1)\bar{v}(t-3)$
-2.214	$\bar{u}^2(t-1)\bar{u}(t-2)$
1.363	$\bar{y}(t-1)\bar{v}(t-3)$
-2.210	$\bar{u}(t-3)\bar{v}(t-3)$
-6.032	$\bar{v}^2(t-2)$
65.71	$\bar{v}(t-1)\bar{v}(t-2)\bar{v}(t-3)$
-10.38	$\bar{u}(t-3)\bar{v}^2(t-1)$
1.904	$\bar{u}(t-1)$

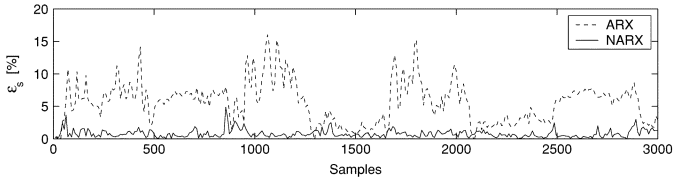

Fig. 5. Isolated mode. Comparison between the NARX and ARX models: relative simulation errors.

to 15% for the latter. Finally, the NARX model provides the correct dc-gain at different FSR operating points.

IV. Conclusion

NARX models has been successfully applied to black box modeling of the PGTA10B1 General Electric-Nuovo Pignone gas turbine operating in isolated and nonisolated mode. The previous nonlinear models outperform the corresponding ARX models and can be usefully employed in simulating different operating conditions of industrial gas turbines. In the identification, particular attention has been devoted to the procedure for structure selection. It has been shown that a careful choice of the ingredients can significantly reduce the complexity and, at the same time, improve the simulation capability of the model.

Acknowledgment

G. Zappa untimely passed away while this paper was under review. The authors would like to remember him and his enthusiasm and courage during this work in difficult times.

References

[1] S. A. Billings and Q. M. Zhu, "Nonlinear model validation using correlation test," *Int. J. Control*, vol. 61, pp. 1107–1120, 1994.

[2] N. Chiras, C. Evans, and D. Rees, "Nonlinear gas turbine modeling using NARMAX structures," *IEEE Trans. Instrumen. Meas.*, vol. 50, no. 4, pp. 893–898, Aug. 2001.

[3] C. Evans, P. J. Fleming, D. C. Hill, J. P. Norton, I. Pratt, D. Rees, and K. Rodriguez-Vazquez, "Application of system identification techniques to aircraft gas-turbine engines," *Control Eng. Pract.*, vol. 9, pp. 135–148, 2001.

[4] G. De Nicolao, C. Rossi, R. Scattolini, and M. Suffriti, "Identification and idle speed control of internal combustion engines," *Control Eng. Pract.*, vol. 7, pp. 1061–1069, 1999.

[5] F. J. Doyle, R. K. Pearson, and B. A. Ogunnaike, *Identification and Control Using Volterra Models*. New York: Springer-Verlag, 2001.

[6] N. Draper and H. Smith, *Applied Regression Analysis*. New York: Wiley, 1981.

[7] U. Forssell and L. Ljung, "Closed-loop identification revisited," *Automatica*, vol. 35, pp. 1215–1241, 1999.

[8] R. Haber and H. Ubenhauen, "Structure identification of nonlinear dynamic systems—A survey on input/output approaches," *Automatica*, vol. 26, pp. 651–677, 1990.

[9] X. Hong and C. J. Harris, "Nonlinear model structure detection using optimum experimental design and orthogonal least squares," *Trans. Neural Netw.*, vol. 12, pp. 435–439, 2001.

[10] W. W. Hung, "Dynamic simulation of gas-turbine generating unit," *Inst. Elect. Eng. Proc. C*, vol. 138, pp. 342–350, 1991.

[11] I. J. Leontaritis and S. A. Billings, "Input-output parametric models for nonlinear systems," *Int. J. Control*, vol. 41, pp. 331–341, 1985.

[12] W. I. Rowen, "Simplified mathematical representations of heavy duty gas turbines," *ASME J. Eng. Power*, vol. 105, pp. 865–869, 1983.

[13] T. Söderström and P. Stoica, *System Identification*. Englewood Cliffs, NJ: Prentice-Hall, 1989.

[14] G. L. Zheng and S. A. Billings, "Qualitative validation and generalization in nonlinear system identification," *Int. J. Control*, vol. 72, pp. 1592–1608, 1999.